Journal of Molecular Spectroscopy 324 (2016) 12–19

Contents lists available at ScienceDirect

Journal of Molecular Spectroscopy

journal homepage: www.elsevier.com/locate/jms

Direct measurement of additional Ar–H_2O vibration–rotation-tunneling bands in the millimeter–submillimeter range

Luyao Zou, Susanna L. Widicus Weaver *

Department of Chemistry, Emory University, 1515 Dickey Drive, Atlanta, GA, USA

ARTICLE INFO

Article history:
Received 19 February 2016
In revised form 12 April 2016
Accepted 18 April 2016
Available online 24 April 2016

Keywords:
Ar–H_2O
VRT
Van der Waals complex

ABSTRACT

Three new weak bands of the Ar–H_2O vibration–rotation-tunneling spectrum have been measured in the millimeter wavelength range. These bands were predicted from combination differences based on previously measured bands in the submillimeter region. Two previously reported submillimeter bands were also remeasured with higher frequency resolution. These new measurements allow us to obtain accurate information on the Coriolis interaction between the 1_{01} and 1_{10} states. Here we report these results and the associated improved molecular constants.

1. Introduction

The intermolecular interaction of van der Waals complexes is crucial to our understanding of the behavior of these complexes, and can be used to simulate the properties of larger systems such as bulk liquids and solvent–solute interactions [1]. Rich information on the intermolecular potential can be deduced from spectroscopic measurement of these complexes [2]. However, the complexity of the vibration–rotation-tunneling (VRT) spectrum arising from the anisotropic intermolecular potential of these complexes is a challenge even for a small dimer system.

Van der Waals complexes can be categorized into the semi-rigid regime or the free-rotor regime based on the barrier height of the intermolecular potential. In the semi-rigid regime, the intermolecular potential is high and the complex can be treated as a whole body with well-defined rotational constants. In the free-rotor regime, on the contrary, one monomer in the complex experiences a low intermolecular potential barrier, and thus rotates almost freely. The effect of the anisotropic intermolecular potential is reflected by the shift and split of rovibrational energy levels of the monomer.

Ar–H_2O dimer is one of the simplest atomic – asymmetric rotor dimers. Nevertheless, its spectrum is complicated. The first two reported VRT bands of Ar–H_2O (0.5–0.8 THz) were assigned by Cohen and coworkers based on a semi-rigid model [3]. The utility of this model was later depreciated after more bands were found both in the far-IR region (1–2 THz) [4,5] and mid-IR region around the ν_3 band (3780 cm^{-1}) [6,7] and ν_2 band (1620 cm^{-1}) [6,8–10] of H_2O. The free-rotor model proposed by Hutson [11] was adopted to assign these bands with success, supporting the fact that the water moiety almost freely rotates. In addition to the Ar–H_2O bands, detection of Ar–D_2O bands in the millimeter region (280–460 GHz) [12] and around multiple D_2O vibration modes, $\nu_1+\nu_2+\nu_3$ (6536 cm^{-1}) [13] and ν_2 (1190 cm^{-1}) [14,15], also supports this dimer being in the free-rotor limit, assuming the intermolecular potential of Ar–D_2O is similar to that of Ar–H_2O. Several transitions were also observed in the microwave range where hyperfine splittings were resolved [16,17]. Combining all of these spectroscopic measurements from the microwave, far-IR, and IR regions, Cohen and Saykally fitted an accurate empirical 3-dimensional potential surface for Ar–H_2O [18].

Here we report the detection of three additional Ar–H_2O bands in the millimeter region. This dataset is complementary to the spectra from Cohen et al. [3]. An energy diagram for Ar–H_2O in the range of this experiment is shown in Fig. 1, highlighting the bands observed by Cohen et al. and the bands detected in the present work. We also remeasured the bands reported by Cohen et al. with higher frequency resolution. Most importantly, to our knowledge, this is the first direct observation of the band origin of the $\Pi(1_{01}) \leftarrow \Sigma(1_{01})$ transitions, the value of which could only be indirectly determined from the difference of other infrared band origins [6]. These new measurements support the free-rotor model of Ar–H_2O, and allow us to determine the band heads with higher accuracy. We present these measurements and the associated analysis herein.

* Corresponding author.
E-mail address: swidicu@emory.edu (S.L. Widicus Weaver).

http://dx.doi.org/10.1016/j.jms.2016.04.010
0022-2852/

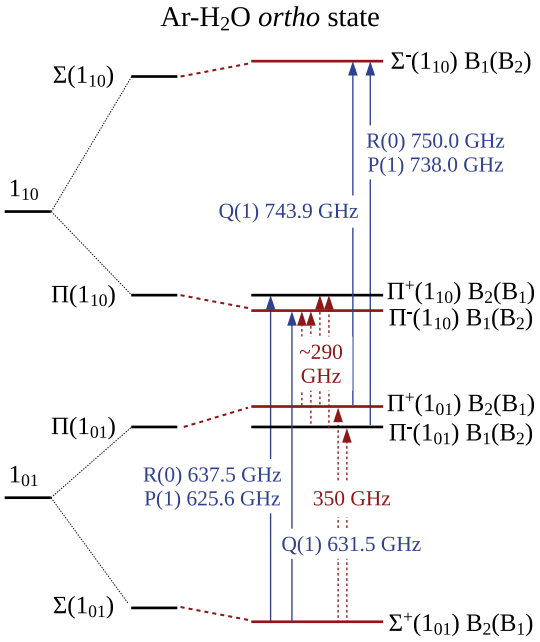

Fig. 1. Ar–H_2O energy diagram in the 1_{01} and 1_{10} states region. Red (dashed) arrows represent the bands detected in the present work. Blue (solid) arrows represent the bands reported by Cohen et al. [3]. These bands are also remeasured in the present work with higher frequency resolution. Band heads are labeled with their approximate transition frequencies. The relative position of these levels is only a qualitative approximation and does not reflect the energy differences between states.

2. Experimental

The Ar–H_2O spectrum was measured in a supersonic jet using a direct absorption multipass millimeter and submillimeter spectrometer. This complex was detected during an experiment designed for probing HO_3, the details of which were reported previously [19]. This follow-up study, by measuring the spectrum of Ar–H_2O, is to confirm the presence of Ar–H_2O in the HO_3 spectrum.

The dimer was readily produced by expanding water vapor in Ar gas (NexAir, UHP) under ambient temperature into the vacuum. The Ar was bubbled through tap water, which was used without further purification. The backing pressure behind the valve was held at 1.3 kTorr above atmosphere. The pulsed valve (Parker Series 9) was driven by a 0.8 ms TTL signal repeated at a rate of 42 Hz.

Millimeter–submillimeter light was generated by passing cm-wave radiation (generated using an Agilent Technology E8257D PSG frequency synthesizer) through a frequency multiplier chain system (Viginia Diodes Inc., S197(c)). The direct absorption spectrum of Ar–H_2O was detected by an InSb hot electron bolometer (QMC Ltd., QFT/XBI). The signal from the detector was recorded digitally via a digitizer card (National Instruments, PCI-5124) and was integrated over the valve opening time as a function of the mil limeter–submillimeter frequency. Integrated intensity was then fitted to a Gaussian line shape. We estimated the uncertainty of the measured frequencies to be 0.1 MHz based on the Doppler width and the slight asymmetry of the line shape that was observed.

The power level at each transition frequency was also measured for the purpose of power normalization. It was achieved by recording the sine waveform of a ±5% depth amplitude modulated signal at these frequencies. These power measurements were recorded during the same run of the experiment to minimize power fluctuations. A sine function was fitted to the waveform and the fitted amplitude was interpreted to be 10% of the power level, assuming a linear correlation between the modulation depth and the radiation power. Power normalization was applied to the integrated intensity of measured spectral lines so that transition intensities were qualitatively comparable.

Other works reported that a slit expansion source may be optimal for dimer yield [3,12,6,14,10]. Nonetheless, we found the pinhole source that had been optimized for HO_3 production [19] yielded sufficiently strong signal for unambiguous detection of Ar–H_2O.

3. Model

The details of the model for Ar–H_2O have been thoroughly discussed in previous works [11,5,12], thus the details are not repeated here. Briefly, since the H_2O molecule in Ar–H_2O rotates nearly freely, it is possible to separate the Hamiltonian of the complex from the Hamiltonian of the monomer. The Hamiltonian of the monomer is then a standard Watson-A type Hamiltonian, and the Hamiltonian of the complex is in the form for a diatomic rotor. The rotational states are labeled with lowercase j_{k_a,k_c} for the monomer, and J and Ω for the complex. The presence of the anisotropic potential arising from the Ar atom splits the rotational states of H_2O into their projections Ω on the monomer–Ar axis. Analogous to the l-doubling in linear molecules, $|\Omega| = 0, 1, 2, \ldots$ are labeled as $\Sigma, \Pi, \Delta, \ldots$ states, respectively. Coriolis interaction further mixes the states of the complex of the same symmetry and H_2O rotational quantum number.

Because of the challenges in developing an effective model for Ar–H_2O, the Hamiltonian and notations used to describe the dimer are not consistent in the literature. In this paper, we chose to follow the model of Cohen et al. [5] to enable direct comparison with their results. Therefore, the rigid rotor energy of the complex is expressed as

$$E = v + B\left[J(J+1) - 2\Omega^2\right] - D\left[J(J+1) - 2\Omega^2\right]^2 + H\left[J(J+1) - 2\Omega^2\right]^3 + L\left[J(J+1) - 2\Omega^2\right]^4 \quad (1)$$

where v is the band head of each water state that is treated as an independent vibrational state. The Coriolis splitting on related energy levels is found by the perturbation matrix

$$\begin{bmatrix} E_1 & H_{\mathrm{Cor}} \\ H_{\mathrm{Cor}} & E_2 \end{bmatrix} \quad (2)$$

where $H_{\mathrm{Cor}} = 2\beta\sqrt{J(J+1)}$ is the Coriolis perturbation Hamiltonian for $j = 1$ states, and E_1 and E_2 (assuming $E_1 < E_2$) are the vibrational energies of two connected states. The shifted energies are

$$E_1' = \frac{1}{2}\left[E_1 + E_2 - (E_2 - E_1)\sqrt{1 + 16J(J+1)\left(\frac{\beta}{E_2 - E_1}\right)^2}\right]$$
$$E_2' = \frac{1}{2}\left[E_1 + E_2 + (E_2 - E_1)\sqrt{1 + 16J(J+1)\left(\frac{\beta}{E_2 - E_1}\right)^2}\right] \quad (3)$$

The lower state corresponds to the negative energy shift, while the upper state corresponds to the positive energy shift.

The symmetry and parity labels are shown in Fig. 1. For each state, the symmetry label outside the parentheses marks even J levels while that inside the parentheses marks odd J levels. We assign arbitrary signs of '+' to the states with $B_2(B_1)$ symmetry, and '−' to the states with $B_1(B_2)$ symmetry. Selection rules allow $B_1 \leftrightarrow B_2$ transitions [12]. Therefore, for P and R branches where $\Delta J = 1$, states with the same sign connect. For Q branches where $\Delta J = 0$, states with opposite signs connect.

Table 1
Transition frequencies of the $\Pi^{+/-}(1_{01}) \leftarrow \Sigma^{+}(1_{01})\, B_2(B_1)$ band of Ar–H_2O. Frequency units are MHz. Experimental uncertainty is estimated to be 0.1 MHz.

	Transition	Obs.	Obs.-calc.		Transition	Obs.	Obs.-calc.
P(17)	16 ← 17	275116.20	−0.07	Q(8)	8 ← 8	342286.93	0.09
P(16)	15 ← 16	277339.86	0.02	Q(9)	9 ← 9	342854.51	0.03
P(15)	14 ← 15	279687.54	0.03	Q(10)	10 ← 10	343448.17	−0.01
P(14)	13 ← 14	282175.49	0.00	Q(11)	11 ← 11	344057.23	−0.08
P(13)	12 ← 13	284819.92	−0.04	Q(12)	12 ← 12	344670.52	−0.12
P(12)	11 ← 12	287637.09	0.09	Q(13)	13 ← 13	345276.39	−0.09
P(11)	10 ← 11	290642.31	0.05	Q(14)	14 ← 14	345862.73	−0.07
P(10)	9 ← 10	293850.95	0.10	Q(15)	15 ← 15	346417.42	0.06
P(9)	8 ← 9	297277.26	0.12	Q(16)	16 ← 16	346927.93	0.11
P(8)	7 ← 8	300934.65	0.11	Q(17)	17 ← 17	347381.93	0.02
P(7)	6 ← 7	304835.44	0.07	R(0)	1 ← 0	345795.42	−0.06
P(6)	5 ← 6	308990.72	0.04	R(1)	2 ← 1	352185.30	−0.06
P(5)	4 ← 5	313410.06	0.00	R(2)	3 ← 2	358850.72	−0.05
P(4)	3 ← 4	318101.52	−0.01	R(3)	4 ← 3	365784.16	−0.01
P(3)	2 ← 3	323071.35	−0.07	R(4)	5 ← 4	372976.06	−0.01
P(2)	1 ← 2	328324.12	−0.08	R(5)	6 ← 5	380415.19	0.00
Q(1)	1 ← 1	339766.22	−0.06	R(6)	7 ← 6	388088.48	0.03
Q(2)	2 ← 2	339924.17	−0.02	R(7)	8 ← 7	395981.20	−0.01
Q(3)	3 ← 3	340157.82	0.00	R(8)	9 ← 8	404077.33	0.00
Q(4)	4 ← 4	340463.38	0.03	R(9)	10 ← 9	412359.38	0.01
Q(5)	5 ← 5	340835.78	0.06	R(10)	11 ← 10	420808.71	−0.03
Q(6)	6 ← 6	341268.87	0.11	R(11)	12 ← 11	429405.85	−0.02
Q(7)	7 ← 7	341755.33	0.10				

Table 2
Transition frequencies of the $\Pi^{+/-}(1_{10}) \leftarrow \Pi^{-}(1_{01})\, B_1(B_2)$ band of Ar–H_2O. Frequency units are MHz. Experimental uncertainty is estimated to be 0.1 MHz.

	Transition	Obs.	Obs.-calc.		Transition	Obs.	Obs.-calc.
P(15)	14 ← 15	209753.90	−0.13	Q(3)	3 ← 3	292739.54	0.00
P(14)	13 ← 14	214423.35	0.00	Q(4)	4 ← 4	293437.84	−0.04
P(13)	12 ← 13	219268.22	0.08	Q(5)	5 ← 5	294320.19	−0.14
P(12)	11 ← 12	224272.48	0.13	R(1)	2 ← 1	303584.79	0.08
P(11)	10 ← 11	229420.27	0.08	R(2)	3 ← 2	309559.69	0.05
P(10)	9 ← 10	234696.27	0.06	R(3)	4 ← 3	315559.60	0.02
P(9)	8 ← 9	240085.57	0.02	R(4)	5 ← 4	321587.51	−0.03
P(8)	7 ← 8	245574.04	−0.02	R(5)	6 ← 5	327647.80	−0.04
P(7)	6 ← 7	251148.48	−0.04	R(6)	7 ← 6	333745.96	−0.08
P(6)	5 ← 6	256796.67	−0.05	R(7)	8 ← 7	339888.77	−0.10
P(5)	4 ← 5	262507.50	−0.07	R(8)	9 ← 8	346083.92	−0.11
P(4)	3 ← 4	268271.22	−0.03	R(9)	10 ← 9	352340.06	−0.08
P(3)	2 ← 3	274079.23	0.00	R(10)	11 ← 10	358666.51	−0.04
P(2)	1 ← 2	279924.40	0.02	R(11)	12 ← 11	365073.25	0.04
Q(1)	1 ← 1	291876.27	0.03	R(12)	13 ← 12	371570.50	0.09
Q(2)	2 ← 2	292220.27	0.00	R(13)	14 ← 13	378168.75	0.10

Table 3
Transition frequencies of the $\Pi^{+/-}(1_{10}) \leftarrow \Pi^{+}(1_{01})\, B_2(B_1)$ band of Ar–H_2O. Frequency units are MHz. Experimental uncertainty is estimated to be 0.1 MHz.

	Transition	Obs.	Obs.-calc.		Transition	Obs.	Obs.-calc.
P(14)	13 ← 14	207269.10	−0.10	Q(1)	1 ← 1	291524.43	0.06
P(13)	12 ← 13	212837.91	0.00	R(1)	2 ← 1	303820.31	0.05
P(12)	11 ← 12	218550.69	0.06	R(2)	3 ← 2	309825.98	0.05
P(11)	10 ← 11	224386.84	0.08	R(3)	4 ← 3	315799.72	0.03
P(10)	9 ← 10	230326.17	0.04	R(4)	5 ← 4	321745.99	−0.01
P(9)	8 ← 9	236349.25	0.02	R(5)	6 ← 5	327671.20	0.01
P(8)	7 ← 8	242437.50	0.02	R(6)	7 ← 6	333583.29	−0.02
P(7)	6 ← 7	248573.41	0.00	R(7)	8 ← 7	339491.97	−0.04
P(6)	5 ← 6	254740.83	−0.03	R(8)	9 ← 8	345408.30	−0.05
P(5)	4 ← 5	260925.14	−0.01	R(9)	10 ← 9	351344.61	−0.03
P(4)	3 ← 4	267113.20	0.00	R(10)	11 ← 10	357314.25	0.02
P(3)	2 ← 3	273293.71	0.03	R(11)	12 ← 11	363331.30	0.01
P(2)	1 ← 2	279457.16	0.01	R(12)	13 ← 12	369410.56	0.06
Q(5)	5 ← 5	289074.93	0.12	R(13)	14 ← 13	375566.92	0.04
Q(4)	4 ← 4	289933.29	0.06	R(14)	15 ← 14	381815.36	0.00
Q(3)	3 ← 3	290633.11	0.06	R(15)	16 ← 15	388170.50	−0.02
Q(2)	2 ← 2	291165.69	0.06	R(16)	17 ← 16	394646.19	−0.03

Table 4
Transition frequencies of the $\Pi^{+/-}(1_{10}) \leftarrow \Sigma^{+}(1_{01})\, B_2(B_1)$ band of Ar–H_2O. Frequency units are MHz. Experimental uncertainty is estimated to be 0.1 MHz. Observed values reported by Cohen et al. [3] (0.5 MHz uncertainty) are also included.

	Transition	Obs.	Obs.-calc.	Obs. [3]		Transition	Obs.	Obs.-calc.	Obs. [3]
P(20)	19 ← 20	564788.83	−0.03	564787.7	Q(10)	10 ← 10	637204.47	−0.01	637204.1
P(19)	18 ← 19	565529.94	0.04	565530.9	Q(11)	11 ← 11	638387.72	−0.03	638388.0
P(18)	17 ← 18	566549.12	−0.01	566550.2	Q(12)	12 ← 12	639685.72	−0.04	639686.1
P(17)	16 ← 17	567847.65	−0.01	567848.6	Q(13)	13 ← 13	641099.85	−0.05	641099.5
P(16)	15 ← 16	569425.55	−0.05	569427.5	Q(14)	14 ← 14	642631.33	−0.05	642632.4
P(15)	14 ← 15	571282.31	−0.04	571283.3	Q(15)	15 ← 15	644281.12	−0.02	644281.8
P(14)	13 ← 14	573416.69	−0.04	573417.7	Q(16)	16 ← 16	646049.72	−0.01	646050.3
P(13)	12 ← 13	575827.14	0.01	575828.1	Q(17)	17 ← 17	647937.19	0.02	647937.5
P(12)	11 ← 12	578511.75	0.01	578512.8	Q(18)	18 ← 18	649942.85	0.02	649942.9
P(11)	10 ← 11	581468.56	0.04	581469.6	Q(19)	19 ← 19	652065.22	−0.01	652065.5
P(10)	9 ← 10	584695.42	0.05	–	R(0)	1 ← 0	637466.72	−0.04	637466.9
P(9)	8 ← 9	588190.25	0.05	588191.4	R(1)	2 ← 1	643791.47	−0.03	643791.6
P(8)	7 ← 8	591951.01	0.05	591952.1	R(2)	3 ← 2	650364.20	−0.06	650364.4
P(7)	6 ← 7	595975.70	0.03	595976.8	R(3)	4 ← 3	657183.52	−0.04	657184.1
P(6)	5 ← 6	600262.42	−0.01	600263.6	R(4)	5 ← 4	664247.81	−0.01	664249.2
P(5)	4 ← 5	604809.42	−0.03	604810.7	R(5)	6 ← 5	671555.47	−0.02	671556.6
P(4)	3 ← 4	609614.99	−0.04	609615.4	R(6)	7 ← 6	679104.95	0.08	679104.3
P(3)	2 ← 3	614677.51	−0.04	614677.8	R(7)	8 ← 7	686894.24	−0.03	686896.1
P(2)	1 ← 2	619995.41	−0.06	619995.6	R(8)	9 ← 8	694921.82	−0.03	694922.0
Q(1)	1 ← 1	631495.57	−0.04	631495.1	R(9)	10 ← 9	703185.60	−0.03	703187.0
Q(2)	2 ← 2	631703.93	−0.02	631703.4	R(10)	11 ← 10	711683.45	−0.03	711684.7
Q(3)	3 ← 3	632016.93	0.01	632017.1	R(11)	12 ← 11	720413.04	0.00	720414.6
Q(4)	4 ← 4	632435.07	0.01	632435.0	R(12)	13 ← 12	729371.63	0.01	729371.1
Q(5)	5 ← 5	632959.13	0.03	632959.0	R(13)	14 ← 13	738556.05	−0.06	738555.8
Q(6)	6 ← 6	633589.98	0.05	633589.9	R(14)	15 ← 14	747962.90	0.03	747963.3
Q(7)	7 ← 7	634328.65	0.03	634328.7	R(15)	16 ← 15	757587.70	0.08	757587.8
Q(8)	8 ← 8	635176.40	0.03	635176.5	R(16)	17 ← 16	767425.22	0.03	767425.6
Q(9)	9 ← 9	636134.53	0.01	636134.6					

Table 5
Transition frequencies of Ar–H_2O $\Sigma^{-}(1_{10})\, B_1(B_2) \leftarrow \Pi^{+/-}(1_{01})$ band. Frequency units are MHz. Experimental uncertainty is estimated to be 0.1 MHz. Observed values reported by Cohen et al. [3] (0.5 MHz uncertainty) are also included.

	Transition	Obs.	Obs.-calc.	Obs. [3]		Transition	Obs.	Obs.-calc.	Obs. [3]
P(10)	9 ← 10	692100.92	0.26	692101.5	Q(6)	6 ← 6	742834.32	0.01	742834.5
P(9)	8 ← 9	696530.41	0.05	696532.2	Q(5)	5 ← 5	743141.15	0.06	743141.2
P(8)	7 ← 8	701135.89	−0.03	701135.9	Q(4)	4 ← 4	743404.16	0.07	743404.2
P(7)	6 ← 7	–	–	705915.4	Q(3)	3 ← 3	743619.40	−0.02	743619.4
P(6)	5 ← 6	710862.99	−0.01	710863.4	Q(2)	2 ← 2	743783.87	0.02	743783.7
P(5)	4 ← 5	715978.38	−0.05	715979.3	Q(1)	1 ← 1	743894.84	−0.04	743894.8
P(4)	3 ← 4	721257.54	−0.07	721259.0	R(1)	2 ← 1	756202.88	−0.06	–
P(3)	2 ← 3	726697.44	−0.01	726699.3	R(2)	3 ← 2	762545.99	−0.01	762545.5
P(2)	1 ← 2	732294.90	0.01	732294.3	R(3)	4 ← 3	769030.48	0.05	769030.3
P(1)	0 ← 1	738047.08	0.11	738046.8	R(4)	5 ← 4	775653.81	−0.01	775654.5
Q(13)	13 ← 13	739871.92	−0.03	–	R(5)	6 ← 5	782413.71	−0.07	782413.3
Q(12)	12 ← 12	740346.67	0.08	–	R(6)	7 ← 6	789307.87	−0.03	789307.3
Q(11)	11 ← 11	740812.25	0.00	740811.7	R(7)	8 ← 7	796333.60	−0.09	796335.7
Q(10)	10 ← 10	741264.36	−0.03	741264.1	R(8)	9 ← 8	803488.30	−0.16	803488.0
Q(9)	9 ← 9	741697.96	−0.02	741697.4	R(9)	10 ← 9	810769.21	−0.08	810769.9
Q(8)	8 ← 8	742107.78	0.08	742107.9	R(10)	11 ← 10	818172.78	−0.03	818176.4
Q(7)	7 ← 7	742488.28	0.06	742488.3					

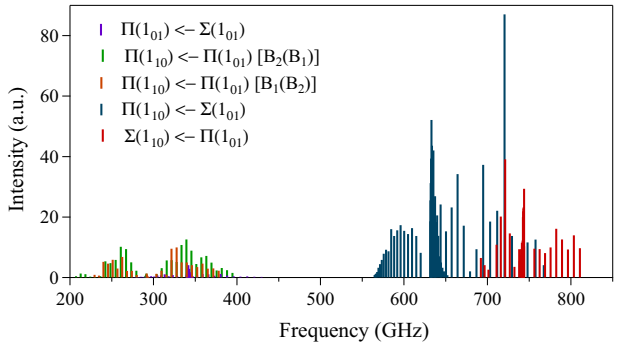

Fig. 2. Full power-normalized stick spectrum of Ar–H_2O from 200 to 800 GHz. (For interpretation of the references to color in this figure legend, the reader is referred to the web version of this article.)

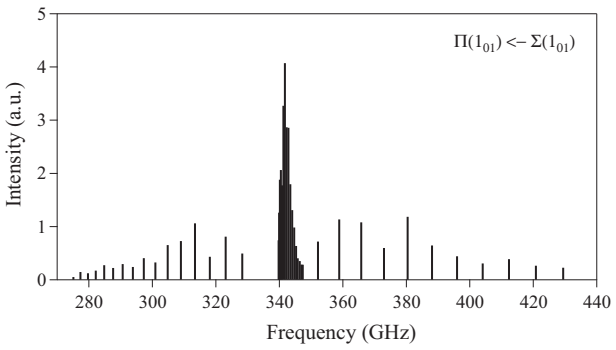

Fig. 3. Power-normalized stick spectrum of the $\Pi^{+/-}(1_{01}) \leftarrow \Sigma^{+}(1_{01})\, B_2(B_1)$ band of Ar–H_2O.

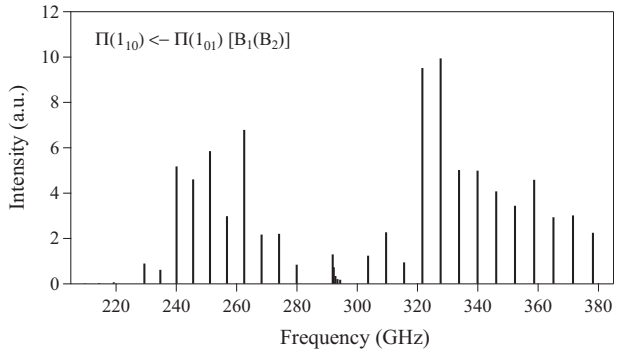

Fig. 4. Power-normalized stick spectrum of the $\Pi^{+/-}(1_{10}) \leftarrow \Pi^{-}(1_{01})$ $B_1(B_2)$ band of Ar–H_2O.

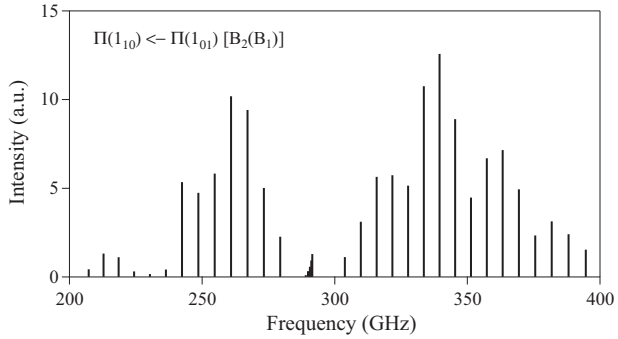

Fig. 5. Power-normalized stick spectrum of the $\Pi^{+/-}(1_{10}) \leftarrow \Pi^{+}(1_{01})$ $B_2(B_1)$ band of Ar–H_2O.

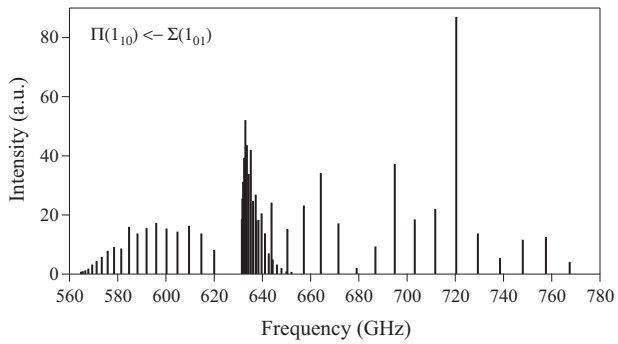

Fig. 6. Power-normalized stick spectrum of the $\Pi^{+/-}(1_{10}) \leftarrow \Sigma^{+}(1_{01})$ $B_2(B_1)$ band of Ar–H_2O.

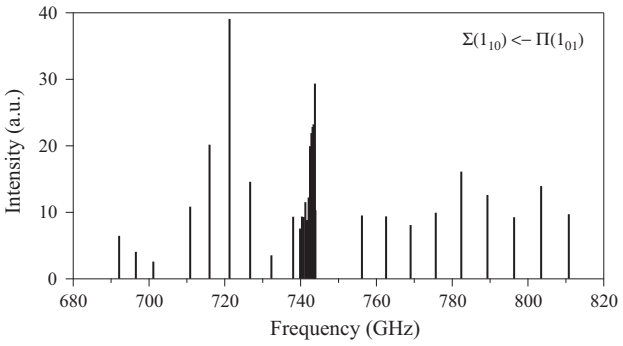

Fig. 7. Power-normalized stick spectrum of Ar–H_2O $\Sigma^{-}(1_{10})$ $B_1(B_2) \leftarrow \Pi^{+/-}(1_{10})$ band.

We fitted the measured transition frequencies to the desired model by a weighted nonlinear least squares algorithm using the "lsqcurvefit" solver in Matlab.[1] Four microwave transitions from a previous study [16] were included in the fit. We assign an uncertainty of 0.005 MHz for the microwave transitions and 0.1 MHz uncertainty for our measurements; the relative weight is proportional to the reciprocal of the square of frequency uncertainties.

4. Result and discussion

4.1. Observed bands

Three new bands of Ar–H_2O *ortho* states were observed in the millimeter wavelength range. Each band has P, Q, and R branches. One band is assigned to the transitions between the $\Pi^{+/-}(1_{01})$ and $\Sigma^{+}(1_{01})$ $B_2(B_1)$ states. The other two are assigned to transitions between the $\Pi(1_{10})$ and $\Pi(1_{01})$ states, in which case the way to group P, Q, and R branches is somewhat arbitrary. We group the branches from the same lower state into one band, i.e., the P and R branches of the $\Pi^{-}(1_{01})$ band connect to the $\Pi^{-}(1_{10})$ state and its Q branch connects to the $\Pi^{+}(1_{10})$ state. Additionally, the two submillimeter bands originally measured by Cohen et al. [3] were remeasured with higher frequency resolution. In the previous experiment, their tunable far-IR lasers had a frequency uncertainty of 0.5 MHz. In our experiment, with high precision multiplier chains, we could constrain the frequency uncertainty of our measurements down to 0.1 MHz. All measured transition frequencies, their assignments, and the observed-calculated residuals from the least squares fit are listed in Tables 1–5. The measurements reported by Cohen et al. [3] are also included for comparison.

The full spectrum is plotted in Fig. 2 where the intensity is proportional to the power-normalized integrated intensity of the measured transition. The stick spectra of each separated band are plotted in Figs. 3–7. Characteristic spectral lines are shown in Fig. 8. The weaker intensities of the $\Pi(1_{01}) \leftarrow \Sigma(1_{01})$ and $\Pi(1_{10}) \leftarrow \Pi(1_{01})$ bands relative to the stronger $\Pi(1_{10}) \leftarrow \Sigma(1_{01})$ and $\Sigma(1_{10}) \leftarrow \Pi(1_{01})$ bands support the assignment of the spectrum under the free-rotor model, because the forbidden transitions between the same H_2O rotational levels are only weakly relaxed in the anisotropic potential of the Ar–H_2O dimer [12].

Despite power normalization, the relative line intensities shown here are still qualitative. The correction is more reliable within a given frequency band from the same multiplier, rather than near the band edges or between different multiplier bands. Near the band edges, the power correction did not fully account for the rapid power drop of multiplier output. In particular, for the undetected P(7) transition in the $\Sigma(1_{10}) \leftarrow \Pi(1_{01})$ band, the majority of radiation power was lost at the frequency of that transition.

4.2. Coriolis interaction

The Coriolis interaction between Σ and Π states is treated as a perturbation between two levels. The analytical eigenvalues of the two-level perturbation matrix are shown in Eq. (3). In previous studies, this interaction is approximated by the first order term of the Taylor series expansion of Eq. (3):

$$E_1' \approx E_1 - 4\beta^2 J(J+1)/(E_2 - E_1)$$
$$E_2' \approx E_2 + 4\beta^2 J(J+1)/(E_2 - E_1) \quad (4)$$

under the assumption that $16\beta^2 J(J+1)/(E_2 - E_1)^2 \ll 1$. In the case of Ar–$H_2O$ *ortho*- states, the splitting of Σ and Π states is on the order of

[1] http://www.mathworks.com/help/optim/ug/lsqcurvefit.html.

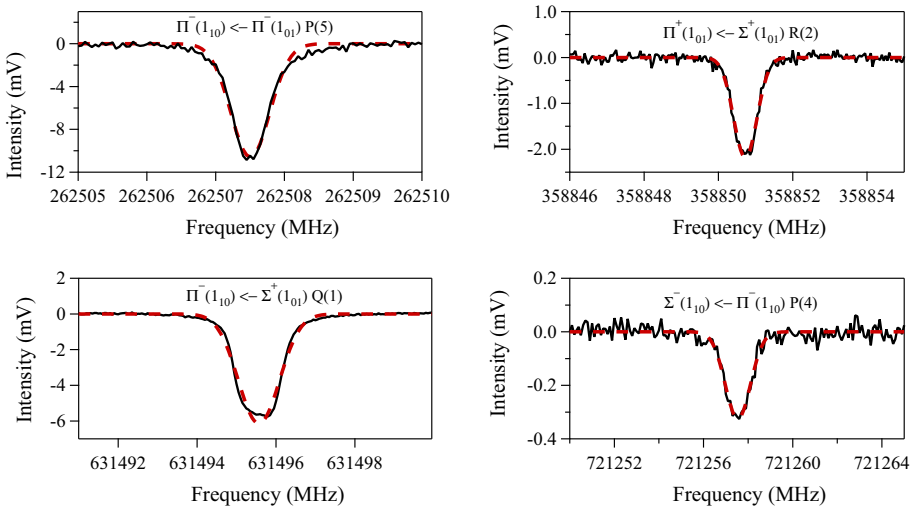

Fig. 8. Characteristic spectral lines. The black solid lines are the experimental integrated intensity, and the red dashed lines are the Gaussian fit. (For interpretation of the references to color in this figure legend, the reader is referred to the web version of this article.)

Table 6
Molecular constants fitted to Ar–H_2O $j = 1$ *ortho* states (rms = 0.060 MHz) and comparison with the results from Cohen and Saykally 1991 [5] (rms = 0.623 MHz). The 1σ uncertainty of each constant is included in the parentheses.

	This work		Cohen and Saykally [5]	
	$\Sigma(1_{01})$	$\Pi(1_{01})$	$\Sigma(1_{01})$	$\Pi(1_{01})$
ν (GHz)	0	345.590524(18)	0	345.587(18)
B (MHz)	3014.7865(17)	2951.6969(70)	3014.783(27)	2951.658(57)
$D(+)$ (kHz)	90.956(13)	115.713(20)	72.616(71)	135.49(40)
$D(-)$ (kHz)	–	114.8240(23)	–	114.76(35)
$H(+)$ (Hz)	−4.316(61)	−1.90(13)	1.25(20)	–
$L(+)$ (mHz)	−2.207(94)	1.85(27)	–	–
β (MHz)	2976.455(14)		2950.84(40)	
	$\Pi(1_{10})$	$\Sigma(1_{10})$	$\Pi(1_{10})$	$\Sigma(1_{10})$
ν (GHz)	637.466766(17)	1083.637495(35)	637.46708(43)	1083.634(18)
B (MHz)	3037.4887(13)	2953.1776(31)	3037.476(15)	2953.224(66)
$D(+)$ (kHz)	60.824(17)	–	60.44(13)	–
$D(-)$ (kHz)	65.149(14)	98.107(76)	51.42(14)	111.75(66)
$H(+)$ (Hz)	−18.796(92)	–	−21.45(28)	–
$H(-)$ (Hz)	−18.449(71)	−14.97(67)	−12.38(32)	−23.9(22)
$L(+)$ (mHz)	−4.54(16)	–	–	–
$L(-)$ (mHz)	−2.49(11)	−9.2(19)	–	–
β (MHz)	2862.862(17)		2880.78(33)	

300 GHz, while β is near 3 GHz. For high J levels (i.e., $J > 10$), the first order approximation starts to introduce a noticeable discrepancy as $16\beta^2 J(J+1)/(E_2 - E_1)^2 > 0.1$. It was shown from our initial test fit that we could only obtain a rms of 2.72 MHz if we only performed a linear fit including the number of constants listed in the analysis of Cohen and Saykally [5]. This rms did not reflect our experimental precision, and the difference between calculated frequencies and experimental frequencies was found to be larger at higher J levels. Therefore, we performed a weighted nonlinear fit using the analytical equations of Coriolis terms (Eq. (3)), instead of approximation the square root term with the first order truncated Taylor series expansion. We observed a significant drop of rms down to 0.30 MHz in the nonlinear fit with the same number of constants used in the linear fit. The fit was furthermore improved by adding higher order centrifugal distortion constants that have statistical significance. We included sextic and octic centrifugal distortion constants for most of the states to achieve a final rms of 0.06 MHz, consistent with the estimated uncertainty of our measurements.

The constants resulting from our nonlinear least squares analysis are listed along with the result from Cohen et al. [5] in Table 6. Here we only fitted the reported transitions from the current study, along with the four microwave transitions from Fraser et al. [16]. Cohen et al. included two additional bands from the ground state to the intermolecular stretching state of Ar–H_2O. However, since each water state is treated as an independent vibrational state, the inclusion of transitions to higher states does not significantly affect the constants determined for lower states. From Table 6, it can bee seen that the accuracy of the water state energies is significantly improved from the observation of direct transitions between these states. For the states unperturbed by Coriolis interaction, the constants in our analysis agree well with the results from Cohen and Saykally [5], but have a higher precision. For the states perturbed by the Coriolis interaction, i.e., $\Sigma^+(1_{01})$, $\Pi^+(1_{01})$, $\Pi^-(1_{10})$, and $\Sigma^-(1_{10})$ states, a systematic discrepancy of the centrifugal distortion constants is observed as compared to the results from Cohen and Saykally [5]. This is because our rigorous Coriolis fit prevents the contamination of the higher order coefficients from the Coriolis splitting into the centrifugal distortion constants. The Taylor series expansion of the Coriolis term in Eq. (3) up to the third order is

Table 7
The contamination arising from the quadratic and cubic terms in the Taylor series expansion of Eq. (5) for Coriolis perturbed states. The contamination is compared to the discrepancy between the analyses of ours and Cohen and Saykally 1991 [5].

Constant	State	Cohen and Saykally [5]	This work	Difference	Contamination (Eq. (5))
$-D$ (kHz)	$\Sigma^+(1_{01})$	−72.616(71)	−90.734(15)	18.340	30.4
$-D$ (kHz)	$\Pi^+(1_{01})$	−135.49(40)	−115.867(20)	−19.777	−30.4
H (Hz)	$\Sigma^+(1_{01})$	1.25(20)	−5.660(28)	5.556	18.0
H (Hz)	$\Pi^+(1_{01})$	–	−1.014(53)	1.014	−18.0
$-D$ (kHz)	$\Pi^-(1_{10})$	−51.42(14)	−64.899(15)	13.729	12.1
$-D$ (kHz)	$\Sigma^-(1_{10})$	−111.75(66)	−97.819(61)	−13.643	−12.1
H (Hz)	$\Pi^-(1_{10})$	−12.38(32)	−19.955(30)	6.069	4.0
H (Hz)	$\Sigma^-(1_{10})$	−23.9(22)	−18.07(23)	−8.93	−4.0

$$\mp\frac{\Delta E}{2}\sqrt{1+16J(J+1)\left(\frac{\beta}{\Delta E}\right)^2}=\frac{\Delta E}{2}\pm\frac{4\beta^2}{\Delta E}J(J+1)\pm\frac{16\beta^4}{\Delta E^3}J^2(J+1)^2\pm\frac{128\beta^6}{\Delta E^5}J^3(J+1)^3 \quad (5)$$

where $\Delta E = E_2 - E_1$ is the difference of corresponding vibrational energies. Substituting the β and ΔE values we obtained in our rigorous analysis, we can evaluate the amount of contamination that arises from the truncated Taylor series expansion. The calculated coefficients of the quadratic and cubic terms in Eq. (5) for each water state are listed in Table 7. These coefficients are expected to agree with the difference between the constants fitted by Cohen and Saykally [5] and by this work, because our fit has removed the effect of this Taylor series expansion in the centrifugal distortion. The results for the 1_{10} states quantitatively agree with the difference. The results for the 1_{01} states only qualitatively agree, indicating that there might be other effects we cannot account for in our analysis. After the removal of this contamination in our nonlinear fit, we found that the centrifugal distortion coefficients of the perturbed and unperturbed states are similar. This similarity indicates that the elongation of the bond length of the complex is not severely affected by the Coriolis effect.

The interpretation of each internal H_2O state energy v from the least squares analysis is model sensitive. The rigid rotor energy term we applied, following Cohen and Saykally [5], is $J(J+1)-2\Omega^2$, i.e., $J(J+1)$ for Σ states and $J(J+1)-2$ for Π states. Other models using $J(J+1)$ [12,15] or $J(J+1)-\Omega^2$ [20] for all states have also been reported. Attention should be paid when comparing results retrieved from these other reports where different models were applied.

5. Conclusion

We have detected three additional vibrational–rotation–tunneling bands of the Ar–H_2O *ortho* state in the millimeter wavelength range. One band is assigned to the $\Pi(1_{01}) \leftarrow \Sigma(1_{01})$ state and the other two are assigned to the $\Pi(1_{10}) \leftarrow \Pi(1_{01})$ states with allowed symmetries. In addition, we confirmed two bands reported by Cohen et al. [3] with higher frequency resolution. The spectrum agrees well with the free-rotor model of Ar–H_2O. The observed bands provide direct measurement of states that were only previously accessible from frequency differences of infrared bands, thus providing additional information of Ar–H_2O energy levels near the minimum of its intermolecular potential.

Acknowledgments

This work is supported by NSF CAREER award CHE-1150492, and start-up funding from Emory University.

References

[1] A.D. Buckingham, P.W. Fowler, J.M. Hutson, Theoretical studies of van der waals molecules and intermolecular forces, Chem. Rev. 88 (6) (1988) 963–988, http://dx.doi.org/10.1021/cr00088a008.
[2] J.M. Hutson, Intermolecular forces from the spectroscopy of van der waals molecules, Ann. Rev. Phys. Chem. 41 (1) (1990) 123–154, http://dx.doi.org/10.1146/annurev.pc.41.100190.001011.
[3] R.C. Cohen, K.L. Busarow, K.B. Laughlin, G.A. Blake, M. Havenith, Y.T. Lee, R.J. Saykally, Tunable far infrared laser spectroscopy of van der Waals bonds: Vibration–rotation–tunneling spectra of Ar–H_2O, J. Chem. Phys. 89 (8) (1988) 4494–4504, http://dx.doi.org/10.1063/1.454789. <http://scitation.aip.org/content/aip/journal/jcp/89/8/10.1063/1.454789>.
[4] R.C. Cohen, K.L. Busarow, Y.T. Lee, R.J. Saykally, Tunable far infrared laser spectroscopy of van der waals bonds: the intermolecular stretching vibration and effective radial potentials for Ar–H_2O, J. Chem. Phys. 92 (1) (1990) 169–177, http://dx.doi.org/10.1063/1.458459. <http://scitation.aip.org/content/aip/journal/jcp/92/1/10.1063/1.458459>.
[5] R.C. Cohen, R.J. Saykally, Multidimensional intermolecular dynamics from tunable far-infrared laser spectroscopy: angular–radial coupling in the intermolecular potential of argon–H_2O, J. Chem. Phys. 95 (11) (1991) 7891–7906, http://dx.doi.org/10.1063/1.461318. <http://scitation.aip.org/content/aip/journal/jcp/95/11/10.1063/1.461318>.
[6] D.J. Nesbitt, R. Lascola, Vibration, rotation, and parity specific predissociation dynamics in asymmetric oh stretch excited Ar–H_2O: a half collision study of resonant v-v energy transfer in a weakly bound complex, J. Chem. Phys. 97 (11) (1992) 8096–8110, http://dx.doi.org/10.1063/1.463431. <http://scitation.aip.org/content/aip/journal/jcp/97/11/10.1063/1.463431>.
[7] S. Kuma, M.N. Slipchenko, T. Momose, A.F. Vilesov, Infrared spectra and intensities of Ar–H_2O and O_2–H_2O complexes in the range of the ν_3 band of H_2O, J. Phys. Chem. A 114 (34) (2010) 9022–9027, http://dx.doi.org/10.1021/jp908450c. pMID: 20669928.
[8] M.J. Weida, D.J. Nesbitt, High resolution mid-infrared spectroscopy of Ar–H_2O: the ν_2 bend region of H_2O, J. Chem. Phys. 106 (8) (1997) 3078–3089, http://dx.doi.org/10.1063/1.473051. <http://scitation.aip.org/content/aip/journal/jcp/106/8/10.1063/1.473051>.
[9] D. Verdes, H. Linnartz, Depletion modulation of Ar–H_2O in a supersonic planar plasma, Chem. Phys. Lett. 355 (5-6) (2002) 538–542, http://dx.doi.org/10.1016/S0009-2614(02)00298-1. <http://www.sciencedirect.com/science/article/pii/S0009261402002981>.
[10] X. Liu, Y. Xu, New rovibrational bands of the Ar–H_2O complex at the ν_2 bend region of H_2O, J. Mol. Spectrosc. 301 (2014) 1–8, http://dx.doi.org/10.1016/j.jms.2014.04.005. <http://www.sciencedirect.com/science/article/pii/S0022285214000903>.
[11] J.M. Hutson, Atom-asymmetric top Van der Waals complexes: angular momentum coupling in Ar–H_2O, J. Chem. Phys. 92 (1) (1990) 157–168, http://dx.doi.org/10.1063/1.458485. <http://scitation.aip.org/content/aip/journal/jcp/92/1/10.1063/1.458485>.
[12] E. Zwart, W.L. Meerts, The submillimeter rotation-tunneling spectrum of Ar–D_2O and Ar–NH_3, Chem. Phys. 151 (3) (1991) 407–418, http://dx.doi.org/10.1016/0301-0104(91)80025-D. <http://www.sciencedirect.com/science/article/pii/030101049180025D>.
[13] K. Didriche, T. Földes, High resolution spectroscopy of the Ar–D_2O and Ar–HDO molecular complexes in the near–infrared range, J. Chem. Phys. 138 (10). doi: http://dx.doi.org/10.1063/1.4794161 <http://scitation.aip.org/content/aip/journal/jcp/138/10/10.1063/1.4794161>.
[14] S. Li, R. Zheng, Y. Zhu, C. Duan, Rovibrational spectra of the Ar–D_2O and Kr–D_2O Van der Waals complexes in the ν_2 bend region of D_2O, J. Mol. Spectrosc. 272 (1) (2012) 27–31, http://dx.doi.org/10.1016/j.jms.2011.12.004. <http://www.sciencedirect.com/science/article/pii/S002228521100292X>.
[15] J.T. Stewart, B.J. McCall, Additional bands of the Ar–D_2O intramolecular bending mode observed using a quantum cascade laser, J. Mol. Spectrosc. 282 (2012) 34–38, http://dx.doi.org/10.1016/j.jms.2012.11.002. <http://www.sciencedirect.com/science/article/pii/S0022285212002160>.
[16] G. Fraser, F. Lovas, R. Suenram, K. Matsumura, Microwave spectrum of Ar–H_2O: dipole moment, isotopic studies, and ^{17}O quadrupole coupling constants, J. Mol. Spectrosc. 144 (1) (1990) 97–112, http://dx.doi.org/10.1016/0022-2852(90)90310-M. <http://www.sciencedirect.com/science/article/pii/002228529090310M>.

[17] T.C. Germann, H.S. Gutowsky, Nuclear hyperfine interactions and dynamic state of H_2O in Ar–H_2O, J. Chem. Phys. 98 (7) (1993) 5235–5238, http://dx.doi.org/10.1063/1.464923. <http://scitation.aip.org/content/aip/journal/jcp/98/7/10.1063/1.464923>.

[18] R.C. Cohen, R.J. Saykally, Determination of an improved intermolecular global potential energy surface for Ar–H_2O from vibration–rotation-tunneling spectroscopy, J. Chem. Phys. 98 (8) (1993) 6007–6030, http://dx.doi.org/10.1063/1.464841. <http://scitation.aip.org/content/aip/journal/jcp/98/8/10.1063/1.464841>.

[19] L. Zou, B.M. Hays, S.L. Widicus Weaver, Weakly bound clusters in astrochemistry? Millimeter and submillimeter spectroscopy of trans-HO_3 and comparison to astronomical observations, J. Phys. Chem. A 120 (5) (2016) 657–667, http://dx.doi.org/10.1021/acs.jpca.5b09624. pMID: 26709536.

[20] S. Suzuki, R.E. Bumgarner, P.A. Stockman, P.G. Green, G.A. Blake, Tunable far-infrared laser spectroscopy of deuterated isotopomers of Ar–H_2O, J. Chem. Phys. 94 (1) (1991) 824–825, http://dx.doi.org/10.1063/1.460308. <http://scitation.aip.org/content/aip/journal/jcp/94/1/10.1063/1.460308>.